OPTICA

36 Hz integral linewidth laser based on a photonic integrated 4.0 m coil resonator

Kaikai Liu,[1,†] Nitesh Chauhan,[1,†] Jiawei Wang,[1] Andrei Isichenko,[1] Grant M. Brodnik,[1] Paul A. Morton,[2] Ryan O. Behunin,[3,4] Scott B. Papp,[5,6] and Daniel J. Blumenthal[1,*]

[1]Department of Electrical and Computer Engineering, University of California Santa Barbara, Santa Barbara, California 93106, USA
[2]Morton Photonics, West Friendship, Maryland 21794, USA
[3]Department of Applied Physics and Materials Science, Northern Arizona University, Flagstaff, Arizona 86011, USA
[4]Center for Materials Interfaces in Research and Applications (¡MIRA!), Northern Arizona University, Flagstaff, Arizona 86011, USA
[5]Department of Physics, University of Colorado Boulder, Boulder, Colorado 80309, USA
[6]Time and Frequency Division 688, National Institute of Standards and Technology, Boulder, Colorado 80305, USA
*Corresponding author: danb@ucsb.edu

Received 17 December 2021; revised 1 June 2022; accepted 20 June 2022; published 7 July 2022

Laser stabilization sits at the heart of many precision scientific experiments and applications, including quantum information science, metrology, and atomic timekeeping. Many of these systems narrow the laser linewidth and stabilize the carrier by use of Pound–Drever–Hall (PDH) locking to a table-scale, ultrahigh quality factor (Q), vacuum spaced Fabry–Perot reference cavity. Integrating these cavities to bring characteristics of PDH stabilization to the chip scale is critical to reducing their size, cost, and weight, and enabling a wide range of portable and system-on-chip applications. We report a significant advance in integrated laser linewidth narrowing, stabilization, and noise reduction by use of a photonic integrated 4.0 m long coil resonator to stabilize a semiconductor laser. We achieve a 36 Hz $1/\pi$-integral linewidth, Allan deviation of 1.8×10^{-13} at 10 ms measurement time, and a 2.3 kHz/s drift—to the best of our knowledge, the lowest integral linewidth and highest stability demonstrated for an integrated waveguide reference cavity. This performance represents over an order of magnitude improvement in integral linewidth and frequency noise over previous integrated waveguide PDH stabilized reference cavities and bulk-optic and integrated injection locked approaches, and over two orders of magnitude improvement in frequency and phase noise than integrated injection locked approaches. Two different wavelength coil designs are demonstrated, stabilizing lasers at 1550 nm and 1319 nm. The resonator is bus-coupled to a 4.0 m long coil, with a 49 MHz free spectral range, mode volume of 1.0×10^{10} μm^3, and 142 million intrinsic Q, fabricated in a CMOS compatible, ultralow loss silicon nitride waveguide platform. Our measurements and simulations show that the thermorefractive noise floor for this particular cavity is reached for frequencies down to 20 Hz in an ambient environment with simple passive vibration isolation and without vacuum or thermal isolation. The thermorefractive noise limited performance is estimated to yield an 8 Hz $1/\pi$-integral linewidth and Allan deviation of 5×10^{-14} at 10 ms, opening a stability regime that heretofore has been available only in fundamentally non-integrated systems. These results demonstrate the potential to bring the characteristics of laboratory-scale stabilized lasers to the integrated, wafer-scale compatible chip scale, and are of interest for a number of applications in quantum technologies and atomic, molecular, and optical physics, and with further developments below 10 Hz linewidth, can be highly relevant to ultralow noise microwave generation.

https://doi.org/10.1364/OPTICA.451635

1. INTRODUCTION

Spectral purity is critical for applications that demand low laser phase noise and high carrier stability, including atomic clocks [1], microwave photonics [2,3], quantum applications [4,5], and energy-efficient coherent communications systems [6]. Lasers with integral linewidths below 1 Hz and Allan deviations better than 10^{-16} over ∼1 s are realized by use of Pound–Drever–Hall (PDH) locking to ultra-stable optical cavities [7–11]. This level of performance is achieved with table-top, vacuum-cavity, ultrahigh finesse resonators that employ sophisticated mirror and athermal designs, and other features to mitigate intrinsic thermal fluctuations [12,13]. Translating qualities of these systems to a photonic integrated, CMOS compatible, wafer-scale platform will enable new generations of precision portable applications as well as systems-on-chip integration [14–16].

Progress towards miniaturization of PDH locked stabilized lasers has centered mainly on bulk-optic reference cavities and

a limited number of integrated cavities. Centimeter-scale whispering gallery mode (WGM) resonators have yielded a fractional frequency noise (FFN) stability of 6×10^{-14} at 100 ms in a thermally and acoustically isolated vacuum enclosure [17]. Injection locking a diode laser to a crystalline WGM resonator achieves a sub-100 Hz integral linewidth and a FFN stability of 4.2×10^{-13} at 10 ms [18], which requires a glass coupling prism for fiber-to-resonator power coupling and a hermetic package to reduce environmental thermal noise. A fused silica micro-cavity stabilized a semiconductor laser to a 25 Hz integral linewidth and a FFN stability of 1×10^{-13} at 20 ms [19,20]. In general, it is desirable to increase the optical mode volume to reduce the various intrinsic thermal noises that scale inversely with mode volume [17,21–23]. Stabilization of a fiber laser to a deep-etched silica waveguide spiral resonator yielded 4×10^{-13} at 0.4 ms and of the order of 100 Hz linewidth [22]. However, new approaches that are less environmentally sensitive and wafer-scale CMOS compatible are critical. Recent CMOS compatible, silicon nitride resonators achieved a $1/\pi$-linewidth reduction from 3.66 kHz to 292 Hz and a carrier stability of 6.5×10^{-13} at 8 ms [24].

In this paper, we report a significant advance in photonic integrated laser stabilization, achieved by locking semiconductor lasers, in both C- and O-bands, to 4.0 m long photonic integrated coil resonators. We measure a 36 Hz $1/\pi$-integral linewidth, 345 Hz β-separation linewidth [25], Allan deviation of 1.8×10^{-13} at 10 ms, and 2.3 kHz/s drift—the lowest integral linewidth and highest stability reported for an integrated reference cavity, to the best of our knowledge. The 36 Hz $1/\pi$-integral linewidth is consistent with the 35 Hz linewidth calculated from the minimum Allan deviation at 1550 nm. We measure the stabilized phase noise at 100 Hz, 1 kHz, and 10 kHz offset from carriers to be −30, −64, and −93 dBc/Hz, respectively. These results represent almost an order of magnitude improvement in integral linewidth and stability and over an order of magnitude lower phase noise than previous PDH locked integrated waveguide reference cavities [23] and between one to two orders of magnitude lower than comparable micro-optic [18] and integrated injection locked [26] laser approaches. Both the 1550 and 1319 nm coil resonators employ 4.0 m long coils, significantly lowering the cavity-intrinsic thermorefractive noise over other designs [23] as well as susceptibility to photothermal noise induced fluctuations. The 1550 nm coil resonator measures a 49.1 MHz free spectral range (FSR), intrinsic 80 million Q, and loaded 55 million Q, and has a $\sim 1.0 \times 10^{10}$ μm^3 mode volume; the 1319 nm coil resonator measures a 48.9 MHz FSR, intrinsic 142 million Q, loaded 71 million Q, and $\sim 0.6 \times 10^{10}$ μm^3 mode volume. We also present numerical modeling of the PDH locking loop noise and the photothermal and thermorefractive noise contributions. We demonstrate that the stabilized frequency noise reaches the thermorefractive noise floor down to 20 Hz frequency offset from the carrier. We estimate the thermorefractive noise limited performance to yield an 8 Hz $1/\pi$-integral linewidth and Allan deviation of 5×10^{-14} at 10 ms, indicating that with mitigation of other noise sources, further performance improvement is possible, opening a stability regime that heretofore has been available only in non-integrated systems. We compare the frequency noise and drift to a Brillouin laser locked to a fused silica microrod Fabry–Perot reference cavity with 25 Hz integral linewidth and show that our linewidth, frequency noise, and Allan deviation performance are comparable. Below 20 Hz, environmental noise dominates, as the resonator is in an ambient environment using simple passive vibration damping isolation and without vacuum or thermal isolation. These results demonstrate the potential to bring the characteristics of laboratory-scale stabilized lasers to the integrated, wafer-scale compatible chip scale, and are of interest for a number of applications in quantum technologies and atomic, molecular, and optical physics (AMO), and with further developments to below 10 Hz linewidth, can be highly relevant to ultralow noise microwave generation and other precision applications.

2. RESULTS

A. Coil Resonator Design and Performance

The Si_3N_4 4.0 m coil waveguide resonator (Fig. S1 in Supplement 1) employs a high aspect ratio waveguide core design, 6 μm wide × 80 nm thick, with a 15 μm thick thermal silicon dioxide lower cladding and 6 μm thick oxide upper cladding deposited by tetraethoxysilane pre-cursor plasma-enhanced chemical vapor deposition (TEOS-PECVD). The coil waveguide spacing is 40 μm, and the minimum bending radius is 9.0 mm. This waveguide design is chosen to provide a low loss high aspect ratio waveguide for the fundamental transverse magnetic (TM) mode to mitigate sidewall scattering loss and to minimize the coil bend radius, waveguide bend loss, and cross talk between coil waveguides [27–29]. The difference in resonator design between the 1550 and 1319 nm resonators is the bus-to-resonator coupler, which for 1550 nm is a directional coupler with a 3.5 μm gap and 3.0 mm coupling length and for 1319 nm is a directional coupler with a 3.5 μm gap and 0.5 mm coupling length. Such a coupler design gives proper coupling for the fundamental TM mode and provides weak coupling for transverse electric modes [30]. The designs of the coil waveguide and directional coupler are described in further detail in Supplement 1 Section 1. To measure the resonator Qs, we use the fiber-extended-cavity semiconductor laser developed by Morton Photonics [2] to probe the resonator and carry out spectral scans with a radio frequency (RF) calibrated fiber Mach–Zehnder interferometer (MZI) as an optical frequency ruler. The 1550 nm resonator is measured to have intrinsic 80 million and 55 million loaded Qs (Fig. S1 in Supplement 1), corresponding to a propagation loss of 0.39 dB/m; the 1319 nm resonator is measured to have intrinsic 142 million and 71 million loaded Qs (Fig. S1 in Supplement 1), corresponding to a propagation loss of 0.16 dB/m. For the coil area and S-bend radius chosen for this design, the 1550 nm bend losses are higher, whereas the 1319 nm bend loss is lower, further away from the critical bend radius, and is scattering loss limited.

B. Laser Stabilization and Frequency Noise Measurements

Laser stabilization is demonstrated by PDH locking a Morton Photonics laser to the 4.0 m long coil resonator and measuring the frequency noise and Allan deviation (Fig. 1). The Morton Photonics laser is a low noise hybrid semiconductor laser with output power as high as 18 dBm and a fundamental linewidth below 100 Hz [2], with 5% of the total power (∼6 dBm) tapped and used for the PDH lock. The coil resonator is mounted on an active temperature controlled stage, inside a passive enclosure on a floating optical table, similar to that described in [24]. The PDH lock requires ∼0.2 mW optical power at the photodetector

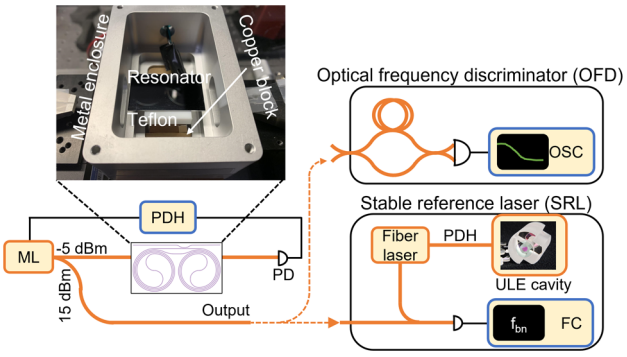

Fig. 1. PDH lock and frequency noise measurement system. A Morton Photonics laser (ML) is locked to the 4-m-long coil resonator in an ambient environment. The resonator sits on a Teflon block, and a thermal-electric cooler underneath the copper block provides mK-level temperature stability. The OFD is used to measure the frequency noise above 1 kHz offset frequency. A Stable Laser Systems (SLS) vacuum reference cavity with ultralow expansion (ULE) glass spacers is used to lock a fiber laser to create a stable reference laser (SRL). The SRL output is photomixed with our stabilized laser output, and the heterodyne beatnote is sent to the frequency counter (FC) for frequency noise measurement below 1 kHz offset frequency. OSC, oscilloscope; PD, photodetector.

to provide a sufficient signal-to-noise ratio (SNR) to overcome other noise sources such as photodetector and shot noise. The PDH locking bandwidth is approximately 1 MHz with a Vescent D2-125 used for the laser servo. For further details of the PDH lock setup, see Supplement 1 Section 2. To measure the frequency noise and laser carrier stability, we use two independent methods. A fiber unbalanced MZI with a 1.026 MHz FSR is used as an optical frequency discriminator (OFD) for self-delayed homodyne laser frequency noise measurement at a frequency offset above 1 kHz [24,31,32]. Since the fiber noise in the MZI dominates at frequencies below 1 kHz offset, we employ a Rock single frequency fiber laser PDH locked to a Stable Laser Systems (SLS) ultralow expansion (ULE) cavity, delivering a Hz-level linewidth output at 1550 nm wavelength with a frequency drift of ~0.1 Hz/s. We refer to this laser as the stable reference laser (SRL). The SRL frequency noise measurement below 1 kHz is performed by photomixing the SRL with our stabilized laser on a high speed photodetector to produce a heterodyne beatnote signal that is measured using a precision frequency counter (Keysight 53200A). The OFD and SRL frequency noise measurements are discussed in detail in Supplement 1 Section 3.

The frequency noise measurements for the 1550 nm coil resonator stabilized laser are shown in Fig. 2, where the OFD and SRL frequency noise measurements are stitched at the 1 kHz frequency offset for both free-running and stabilized lasers. From the frequency noise spectrum, the $1/\pi$-integral linewidth and β-separation linewidth can be calculated to evaluate the laser noise and linewidth performance [11,18,25]. The $1/\pi$-integral linewidths for the free-running and stabilized lasers in Fig. 2(a) are 1.3 kHz and 36 Hz, respectively. The β-separation linewidths for the free-running and stabilized lasers are also calculated to be

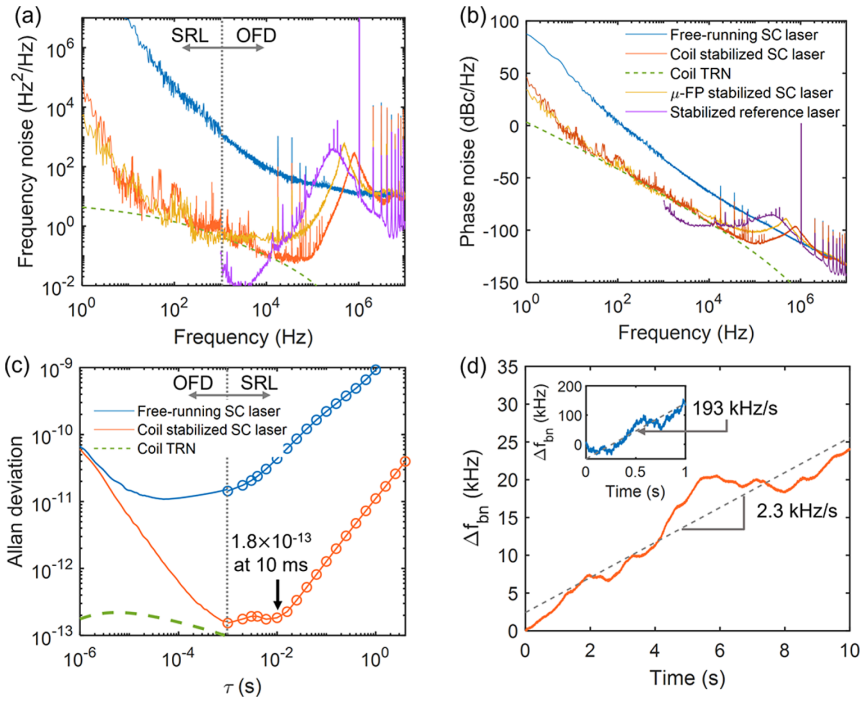

Fig. 2. 1550 nm integrated 4.0 m coil resonator stabilized laser frequency noise, Allan deviation, and beatnote frequency drift. (a) OFD and SRL frequency noise measurements for the free-running and coil stabilized laser and comparison to performance of a laser stabilized to a bulk-optic fused silica microrod Fabry–Perot cavity (μ-FP). SRL frequency noise above 1 kHz is included to show properties of the laser used for heterodyne beatnote measurements indicated by SRL region of noise plot. OFD regions denote frequency noise data taken with a fiber MZI frequency discriminator, and SRL regions denote frequency noise data taken by beating the coil stabilized laser with a ~1 Hz linewidth cavity stabilized reference laser. OFD, optical frequency discriminator; SRL, stabilized reference laser. The curve legend is the same as in (b). (b) The corresponding single sideband (SSB) phase noise is calculated from the frequency noise in (a). (c) The Allan deviation is estimated based on the heterodyne signal frequency recorded by a frequency counter at an averaging time τ above 1 ms with the linear drift removed. The stabilized laser measures an Allan deviation of 1.8×10^{-13} at 10 ms. (d) The beatnote frequency drift $[\Delta f_{bt} = f_{bn}(t) - f_{bn}(0)]$ is measured on the frequency counter with a gatetime of 1 ms, where $f_{bn}(0)$ is ~54 MHz for the free-running and ~61 MHz for the stabilized laser. OFD, optical frequency discriminator; SRL, stable reference laser; SC laser, semiconductor laser; TRN, thermorefractive noise.

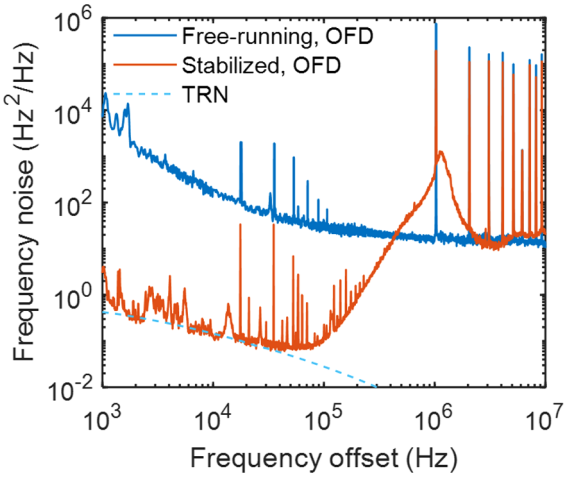

Fig. 3. O-band 1319 nm laser stabilization with the coil waveguide resonator and frequency noise measured by the optical frequency discriminator (OFD) method. The stabilized laser reaches the thermorefractive noise limit from 1 to 50 kHz.

91 kHz and 345 Hz, respectively (see Supplement 1 Section 3 and Fig. S4 for $1/\pi$-integral and β-separation linewidth calculations). The Allan deviation calculated from the OFD and SRL frequency noise measurements for the stabilized laser reaches a minimum of 1.8×10^{-13} at 10 ms [Fig. 2(c)], representing an improvement of over two orders of magnitude over the free-running laser. The stabilized laser's frequency noise spectrum falls onto the resonator-intrinsic thermorefractive noise from 50 kHz down to 20 Hz offset, as shown in Fig. 2(a), whereas below 20 Hz, the resonator in the ambient environment suffers from environmental noise such as thermal fluctuation noise. Figure 2(d) shows the measurement of the coil resonator's linear drift of 2.3 kHz/s, a 100× reduction compared to that of the free-running laser (193 kHz/s). We also demonstrate this laser stabilization at the O-band (1319 nm) as shown in Fig. 3, where the stabilized laser measured by OFD reaches the thermorefractive noise limit from 1 to 50 kHz. In Fig. 2(a), we also compare these results to the frequency noise of the laser locked to a billion Q fused microrod Fabry–Perot cavity (μ-FP) [20] and a fiber laser locked to the SLS cavity, demonstrating that our coil resonator stabilized laser achieves comparable performance. Single sideband phase noise is calculated and plotted in Fig. 2(b), where the coil resonator stabilized laser phase noise is measured to be −30 dBc/Hz at 100 Hz, −64 dBc/Hz at 1 kHz, and −93 dBc/Hz at 10 kHz.

The β-separation linewidth includes noise contributions to the shoulders of the Gaussian line shape, which occur at close-to-carrier frequencies. The $1/\pi$-integral linewidth accounts for phase noise components from high frequencies towards the frequency where the integration area is $1/\pi$, which in our case is 36 Hz. This point (36 Hz) represents the random walk of the laser phase over a 2π interval since this is a single sideband noise measurement. The $1/\pi$-integral accounts for the noise power that contributes the linewidth wings down to 36 Hz offset from the carrier. We confirm that the $1/\pi$-integral linewidth is self-consistent with the measured minimum Allan deviation at 1550 nm carrier frequency, which corresponds to an approximate 35 Hz linewidth. For this stabilized laser, the difference in linewidth calculations is expected, as the close-to-carrier noise is dominated by environmental and electronic noise as well as thermal drift. Such noise sources are reduced in state of the art stabilized laser systems using cryogenically cooled, vacuum isolated enclosures and designs that incorporate vacuum core cavities, in which case the β-separation and $1/\pi$-integral linewidths will converge. In general, the linewidth strongly depends on the averaging time relevant for a particular application, where the laser drift eventually dominates the linewidth after the minimum Allan deviation.

C. Frequency Noise Analysis

To understand the stabilized laser frequency noise and limitations at 1550 nm, we simulate the noise contributions such as photodetector noise and shot noise in the locking loop and photothermal noise and thermorefractive noise in the coil resonator. The reference cavity Q plays a critical role in determining the stabilized laser performance. For example, the SNR of the frequency discrimination of the laser noise against other noise sources such as photodetector noise, shot noise, and electronic noise is proportional to Q and the optical power incident on the photodetector [33]. With our resonator with an 80 million intrinsic Q and approximately 0.2 mW optical power incident on the photodetector (Thorlabs PDB470C), the photodetector noise and shot noise are estimated to be 4×10^{-3} and 6×10^{-4} Hz^2/Hz, respectively (see Supplement 1 Section 2), which do not pose a noise limit on the PDH lock performance. We also calculate that photothermal noise, which is estimated to be 2×10^{-5} Hz^2/Hz (see Supplement 1 Section 2), is not a dominant contribution since both photothermal noise and thermorefractive noise scale inversely with the optical mode volume. We model the thermorefractive noise following [34,35] and determine that for this 4.0 m long coil resonator with a 1.0×10^{10} μm^3 mode volume, the thermorefractive noise reaches 1.2 Hz^2/Hz at 1 Hz offset as shown in the green dashed curve in Fig. 2(a). There are additional mechanisms that can convert optical power fluctuations in the coil resonator into frequency noise, such as Kerr and photo-elastic effects. The Kerr effect for this design is several orders of magnitude smaller than the thermal effect at low frequencies within the thermal bandwidth [36,37]. Recently, we reported that the photothermal effect in a much smaller resonator (7.4 cm long) can be dominant below 10 kHz frequency offset [24,38]. Reducing the environmental noise for this coil resonator and increasing the cavity Q, we estimate the stabilized laser frequency noise can reach a thermorefractive noise limited 8 Hz $1/\pi$-integral linewidth.

3. SUMMARY AND DISCUSSION

We report a significant advance in photonic integrated laser stabilization, achieved by using a 4.0 m coil silicon nitride waveguide resonator to PDH stabilize a fiber-extended cavity semiconductor laser. The coil resonator is a bus-coupled 4.0 m long waveguide fabricated in the ultralow loss silicon nitride CMOS compatible platform [15,29,30]. We measure a $1/\pi$-integral linewidth of 36 Hz, β-separation linewidth of 345 Hz, and Allan deviation of 1.8×10^{-13} at 10 ms—the lowest integral linewidth and highest stability reported for an all-waveguide design, to the best of our knowledge. We demonstrate that the stabilized laser frequency noise reaches the resonator thermorefractive noise limit from 50 kHz down to 20 Hz. The 1.8×10^{-13} Allan deviation for the 193 THz carrier yields a 35 Hz linewidth, consistent with the $1/\pi$-integral 36 Hz linewidth. The consistency between these measurements enables us to determine that carrier jitter is the

Table 1. Comparison of Non-vacuum Miniaturized and Integrated Cavities to this Work

Cavity	LockMethod	$1/\pi$ Integral Linewidth	β-Separation Linewidth	AllanDeviation	PhaseNoise (dBc/Hz) at 0.1/1/10 kHz
Integrated spiral resonator [23]	PDH lock	312 Hz[a]	2.5 kHz[a]	3.9×10^{-13} at 0.4 ms 1×10^{-12} at 10 ms	–16/–53/–77
Integrated SiN ring resonator [26]	Injection lock	2.3 kHz[a]	5.6 kHz[a]	–	–/–25[a]/–64[a]
Bulk optic WGM resonator [18]	Injection lock	50 Hz	2.9 kHz[a]	4.2×10^{13} at 10 ms	–18[a]/–46[a]/–75[a]
Bulk optic silica microrod [20]	PDH lock	25 Hz	–	1×10^{-13} at 20 ms	–40[a]/–75[a]/–87[a]
This work	PDH lock	36 Hz	345 Hz	1.8×10^{-13} at 10 ms	–30/–64/–93

[a]Calculated from the published frequency noise spectra.

major contribution to the 36 Hz integral linewidth out to 10 ms. After 10 ms, the linewidth is dominated by drift, which is measured to be 2.3 kHz/s. Additionally, we report stabilization of a laser in the O-band, reaching the thermorefractive noise limit from 40 kHz down to 1 kHz, where the lower frequency measurement is limited by our optical frequency discrimination method and lack of an ultra-stable reference source at this wavelength.

Table 1 summarizes these results in comparison with lasers based on vacuum-free miniaturized and integrated cavities. The performance of the PDH coil stabilized laser approaches that of a bulk-optic fused silica micro-cavity Fabry–Perot resonator used to PDH stabilize a semiconductor laser to 25 Hz integral linewidth and 3×10^{-13} Allan deviation at 20 ms [20]. In comparison to an integrated waveguide spiral resonator used to PDH lock a fiber laser [23], this work achieves an order of magnitude reduction in integral linewidth and Allan deviation and over an order of magnitude reduction in phase noise at 0.1, 1.0, and 10 kHz offset from carrier frequencies. An alternative approach to PDH locking is the widely studied injection locked technique [18], where the reference resonator is located inside the laser cavity, providing direct optical feedback. We report comparable $1/\pi$ integral linewidth and Allan deviation to a bulk-optic WGM resonator injection locked laser [18], and an order of magnitude improvement in β-separation linewidth and more than two orders of magnitude improvement in frequency/phase noise performance out to 10 kHz. In comparison to an integrated silicon photonic injection locked laser, we achieve two orders of magnitude improvement in integral linewidth and phase noise [26]. The frequency noise, phase noise, and Allan deviation (ADEV) data used to generate Table 1 are discussed in Supplement 1 Section 4, and shown in Fig. S5 in Supplement 1 Section 4.

One advantage of the integrated coil resonator over bulk-optic and table-scale designs is that the optical mode volume can be increased while delivering high Q and maintaining a compact footprint. There is a trade-off between the coil length (mode volume) and the resonator Q for a given waveguide loss including the bend losses for that waveguide design and operating wavelength. The low waveguide mode confinement used in this work achieves low loss and high Q while the critical bend radius sets the coil area. The choice of 4.0 m allows us to maximize the resonator volume for a desired mode loss and resonator Q required for laser stabilization, while at the same time satisfying other constraints imposed by bend losses including fitting the device to within a single lithographic field. Future work includes increasing optical waveguide confinement while maintaining low propagation loss to reduce the critical bending radius and hence the coil area. An advantage of the PDH configuration is that only a small amount of power (determined by the loop noise sources and required SNR) need be tapped from the laser output and injected into the coil reference cavity. Keeping the power to a minimum in the coil resonator reduces photothermal noise. Our frequency noise measurement technique is able to validate that the thermorefractive limit is reached down to 20 Hz. However, below 20 Hz, environmental noise dominates the thermorefractive components. In terms of the thermorefractive noise floor, our simulations for this resonator design are based on optical parameters such as refractive index and thermo-optic coefficient and the material thermal parameters such as conductivity, density, and heat capacity, leading to an estimate for the coil resonator thermorefractive noise spectrum. The thermorefractive noise spectrum does not provide an explanation for the flat frequency noise spectrum from 10 to 100 kHz, and future work will focus on noise sources that contribute to this frequency band.

Based on the above estimates, the thermorefractive noise limited performance for this coil is an 8 Hz $1/\pi$-integral linewidth and Allan deviation of 5×10^{-14} at 10 ms. Further improvements can be achieved by increasing the resonator Q [29,30] and length and reducing the coil area. Increased Q will result in a higher SNR for the PDH lock, and improved packaging will reduce environmental induced frequency noise. Since the low-confinement optical mode is mostly distributed in the silicon dioxide cladding whose thermo-optic coefficient is around $1 \times 10^{-5}\ 1/K$, the corresponding thermal coefficient of the resonance shift from the ambient temperature change is approximately 1 MHz/mK, and thus temperature isolation, control, or athermal design approaches will be needed. The frequency noise sensitivity for vibration and acoustic noise needs to be characterized, and mitigation can be incorporated in future package design [20]. Other areas of improvement include an increase in coil length, incorporation of athermal designs [39], and dual waveguide mode precision temperature measurements [38], which can be combined for feedback loop noise engineering. Looking forward, this silicon nitride fully planar design can be integrated with a wide range of lasers and components that have been demonstrated in this platform [15]. These results show promise to bring the characteristics of table-top and miniaturized ultrahigh Q resonators to planar all-waveguide solutions that are CMOS wafer-scale compatible, and bring benefits to applications for a wide range (including mobile) precision applications including atomic clocks, microwave photonics, quantum sensing, metrology, and computing applications, and energy-efficient coherent communications systems.

Funding. National Institute of Standards and Technology (NIST); Advanced Research Projects Agency—Energy ARPA-E FRESCO (DE-AR0001042); Defense Advanced Research Projects Agency DARPA GRYPHON (HR0011-22-2-0008).

Acknowledgment. Andrei Isichenko acknowledges the support from the National Defense Science and Engineering Graduate (NDSEG) Fellowship

Program. The views and conclusions contained in this document are those of the authors and should not be interpreted as representing official policies of DARPA, ARPA-E, or the U.S. Government.

Disclosures. The authors declare no conflicts of interest.

Data availability. Data underlying the results presented in this paper are not publicly available at this time but may be obtained from the authors upon reasonable request.

Supplemental document. See Supplement 1 for supporting content.

†These authors contributed equally to this paper.

REFERENCES

1. A. D. Ludlow, M. M. Boyd, J. Ye, E. Peik, and P. O. Schmidt, "Optical atomic clocks," Rev. Mod. Phys. **87**, 637–701 (2015).
2. P. A. Morton and M. J. Morton, "High-power, ultra-low noise hybrid lasers for microwave photonics and optical sensing," J. Lightwave Technol. **36**, 5048–5057 (2018).
3. J. Li, H. Lee, and K. J. Vahala, "Microwave synthesizer using an on-chip Brillouin oscillator," Nat. Commun. **4**, 2097 (2013).
4. A. Orieux and E. Diamanti, "Recent advances on integrated quantum communications," J. Opt. **18**, 083002 (2016).
5. G. Zhang, J. Y. Haw, H. Cai, F. Xu, S. M. Assad, J. F. Fitzsimons, X. Zhou, Y. Zhang, S. Yu, J. Wu, W. Ser, L. C. Kwek, and A. Q. Liu, "An integrated silicon photonic chip platform for continuous-variable quantum key distribution," Nat. Photonics **13**, 839–842 (2019).
6. D. J. Blumenthal, H. Ballani, R. O. Behunin, J. E. Bowers, P. Costa, D. Lenoski, P. A. Morton, S. Papp, and P. T. Rakich, "Frequency stabilized links for coherent WDM fiber interconnects in the datacenter," J. Lightwave Technol. **38**, 3376–3386 (2020).
7. R. W. P. Drever, J. L. Hall, F. V. Kowalski, J. Hough, G. M. Ford, A. J. Munley, and H. Ward, "Laser phase and frequency stabilization using an optical resonator," Appl. Phys. B **31**, 97–105 (1983).
8. Y. Y. Jiang, A. D. Ludlow, N. D. Lemke, R. W. Fox, J. A. Sherman, L.-S. Ma, and C. W. Oates, "Making optical atomic clocks more stable with 10–16 -level laser stabilization," Nat. Photonics **5**, 158–161 (2011).
9. T. Kessler, C. Hagemann, C. Grebing, T. Legero, U. Sterr, F. Riehle, M. J. Martin, L. Chen, and J. Ye, "A sub-40-mHz-linewidth laser based on a silicon single-crystal optical cavity," Nat. Photonics **6**, 687–692 (2012).
10. S. Hirata, T. Akatsuka, Y. Ohtake, and A. Morinaga, "Sub-hertz-linewidth diode laser stabilized to an ultralow-drift high-finesse optical cavity," Appl. Phys. Express **7**, 022705 (2014).
11. D. G. Matei, T. Legero, S. Häfner, C. Grebing, R. Weyrich, W. Zhang, L. Sonderhouse, J. M. Robinson, J. Ye, F. Riehle, and U. Sterr, "1.5 μm lasers with sub-10 mHz linewidth," Phys. Rev. Lett. **118**, 263202 (2017).
12. K. Numata, A. Kemery, and J. Camp, "Thermal-noise limit in the frequency stabilization of lasers with rigid cavities," Phys. Rev. Lett. **93**, 250602 (2004).
13. M. Notcutt, L.-S. Ma, A. D. Ludlow, S. M. Foreman, J. Ye, and J. L. Hall, "Contribution of thermal noise to frequency stability of rigid optical cavity via Hertz-linewidth lasers," Phys. Rev. A **73**, 031804 (2006).
14. M. H. P. Pfeiffer, J. Liu, A. S. Raja, T. Morais, B. Ghadiani, and T. J. Kippenberg, "Ultra-smooth silicon nitride waveguides based on the Damascene reflow process: fabrication and loss origins," Optica **5**, 884–892 (2018).
15. D. J. Blumenthal, R. Heideman, D. Geuzebroek, A. Leinse, and C. Roeloffzen, "Silicon nitride in silicon photonics," Proc. IEEE **106**, 2209–2231 (2018).
16. D. Marpaung, J. Yao, and J. Capmany, "Integrated microwave photonics," Nat. Photonics **13**, 80–90 (2019).
17. J. Alnis, A. Schliesser, C. Y. Wang, J. Hofer, T. J. Kippenberg, and T. W. Hänsch, "Thermal-noise-limited crystalline whispering-gallery-mode resonator for laser stabilization," Phys. Rev. A **84**, 011804 (2011).
18. W. Liang, V. S. Ilchenko, D. Eliyahu, A. A. Savchenkov, A. B. Matsko, D. Seidel, and L. Maleki, "Ultralow noise miniature external cavity semiconductor laser," Nat. Commun. **6**, 7371 (2015).
19. W. Zhang, F. Baynes, S. A. Diddams, and S. B. Papp, "Microrod optical frequency reference in the ambient environment," Phys. Rev. Appl. **12**, 024010 (2019).
20. W. Zhang, L. Stern, D. Carlson, D. Bopp, Z. Newman, S. Kang, J. Kitching, and S. B. Papp, "Ultranarrow linewidth photonic-atomic laser," Laser Photon. Rev. **14**, 1900293 (2020).
21. J. Lim, A. A. Savchenkov, E. Dale, W. Liang, D. Eliyahu, V. Ilchenko, A. B. Matsko, L. Maleki, and C. W. Wong, "Chasing the thermodynamical noise limit in whispering-gallery-mode resonators for ultrastable laser frequency stabilization," Nat. Commun. **8**, 8 (2017).
22. G. Huang, E. Lucas, J. Liu, A. S. Raja, G. Lihachev, M. L. Gorodetsky, N. J. Engelsen, and T. J. Kippenberg, "Thermorefractive noise in silicon-nitride microresonators," Phys. Rev. A **99**, 061801 (2019).
23. H. Lee, M.-G. Suh, T. Chen, J. Li, S. A. Diddams, and K. J. Vahala, "Spiral resonators for on-chip laser frequency stabilization," Nat. Commun. **4**, 2468 (2013).
24. K. Liu, J. H. Dallyn, G. M. Brodnik, A. Isichenko, M. W. Harrington, N. Chauhan, D. Bose, P. A. Morton, S. B. Papp, R. O. Behunin, and D. J. Blumenthal, "Photonic circuits for laser stabilization with ultra-low-loss and nonlinear resonators," arXiv:2107.03595 (2021).
25. G. Di Domenico, S. Schilt, and P. Thomann, "Simple approach to the relation between laser frequency noise and laser line shape," Appl. Opt. **49**, 4801–4807 (2010).
26. W. Jin, Q.-F. Yang, L. Chang, B. Shen, H. Wang, M. A. Leal, L. Wu, M. Gao, A. Feshali, M. Paniccia, K. J. Vahala, and J. E. Bowers, "Hertz-linewidth semiconductor lasers using CMOS-ready ultra-high- Q microresonators," Nat. Photonics **15**, 346–353 (2021).
27. J. F. Bauters, M. J. R. Heck, D. John, *et al.*, "Ultra-low-loss high-aspect-ratio Si3N4 waveguides," Opt. Express **19**, 3163–3174 (2011).
28. D. T. Spencer, J. F. Bauters, M. J. R. Heck, and J. E. Bowers, "Integrated waveguide coupled Si_3N_4 resonators in the ultrahigh-Q regime," Optica **1**, 153–157 (2014).
29. M. W. Puckett, K. Liu, N. Chauhan, Q. Zhao, N. Jin, H. Cheng, J. Wu, R. O. Behunin, P. T. Rakich, K. D. Nelson, and D. J. Blumenthal, "422 Million intrinsic quality factor planar integrated all-waveguide resonator with sub-MHz linewidth," Nat. Commun. **12**, 934 (2021).
30. K. Liu, N. Jin, H. Cheng, N. Chauhan, M. W. Puckett, K. D. Nelson, R. O. Behunin, P. T. Rakich, and D. J. Blumenthal, "Ultralow 0.034 dB/m loss wafer-scale integrated photonics realizing 720 million Q and 380 μW threshold Brillouin lasing," Opt. Lett. **47**, 1855–1858 (2022).
31. P. Horak and W. H. Loh, "On the delayed self-heterodyne interferometric technique for determining the linewidth of fiber lasers," Opt. Express **14**, 3923–3928 (2006).
32. S. Gundavarapu, G. M. Brodnik, M. Puckett, T. Huffman, D. Bose, R. Behunin, J. Wu, T. Qiu, C. Pinho, N. Chauhan, J. Nohava, P. T. Rakich, K. D. Nelson, M. Salit, and D. J. Blumenthal, "Sub-hertz fundamental linewidth photonic integrated Brillouin laser," Nat. Photonics **13**, 60–67 (2018).
33. E. D. Black, "An introduction to Pound–Drever–Hall laser frequency stabilization," Am. J. Phys. **69**, 79–87 (2000).
34. M. L. Gorodetsky and I. S. Grudinin, "Fundamental thermal fluctuations in microspheres," J. Opt. Soc. Am. B **21**, 697–705 (2004).
35. J. H. Dallyn, K. Liu, M. W. Harrington, G. M. Brodnik, P. T. Rakich, D. J. Blumenthal, and R. O. Behunin, "Thermal and driven noise in Brillouin lasers," Phys. Rev. A **105**, 043506 (2022).
36. J. Liu, G. Huang, R. N. Wang, J. He, A. S. Raja, T. Liu, N. J. Engelsen, and T. J. Kippenberg, "High-yield wafer-scale fabrication of ultralow-loss, dispersion-engineered silicon nitride photonic circuits," Nat. Commun. **12**, 2236 (2020).
37. K. Ikeda, R. E. Saperstein, N. Alic, and Y. Fainman, "Thermal and Kerr nonlinear properties of plasma-deposited silicon nitride/silicon dioxide waveguides," Opt. Express **16**, 12987–12994 (2008).
38. Q. Zhao, M. W. Harrington, A. Isichenko, K. Liu, R. O. Behunin, S. B. Papp, P. T. Rakich, C. W. Hoyt, C. Fertig, and D. J. Blumenthal, "Integrated reference cavity with dual-mode optical thermometry for frequency correction," Optica **8**, 1481–1487 (2021).
39. Q. Zhao, R. O. Behunin, P. T. Rakich, N. Chauhan, A. Isichenko, J. Wang, C. Hoyt, C. Fertig, M. H. Lin, and D. J. Blumenthal, "Low-loss low thermo-optic coefficient Ta_2O_5 on crystal quartz planar optical waveguides," APL Photon. **5**, 116103 (2020).